Diverse Embedment Model for Steel Fiber-Reinforced Concrete in Tension: Model Development

by Seong-Cheol Lee, Jae-Yeol Cho, and Frank J. Vecchio

An analysis model is presented for calculating the response of steel fiber-reinforced concrete (SFRC) members subjected to tension. To predict the tensile stress of fibers across a crack, the pullout behavior of a single fiber with both sides embedded in cracked concrete is analytically investigated, considering both frictional bond behavior and mechanical anchorage effects. Thus, the proposed Diverse Embedment Model (DEM) can be applied to end-hooked and straight fibers. The model is derived with consideration given to all possible fiber orientations and embedment lengths and as influenced by the member's finite dimensions. The details of the experimental verification for the proposed analysis model, including the proposed fiber orientation factors, are presented and discussed in an accompanying paper.

INTRODUCTION

Fibers are increasingly being used in concrete structures to compensate for concrete's weak and brittle tensile behavior relative to its compression response. One of the most beneficial aspects of the use of fibers in concrete structures is that non-brittle behavior after concrete cracking can be achieved with fibers. The typical tensile stress and crack width relationships for normal concrete (NC) and fiber-reinforced concrete (FRC) are compared in Fig. 1. As indicated in this figure, the tensile stress sustainable in NC rapidly decreases immediately after cracking. In FRC, on the other hand, fibers crossing the crack interfaces significantly contribute to the load-carrying mechanism so that considerable tensile stress, being the sum of the tensile resistance provided by fibers and tension softening of the concrete matrix, respectively, can be achieved even with large crack widths. Therefore, the enhanced tensile stress behavior attainable with fibers should be realistically evaluated to accurately predict the post-cracking response of FRC.

Several researchers have made contributions to the development of analytical models for the uniaxial tensile behavior of FRC. Considering the random distribution of fiber embedment length, Marti et al.[2] derived a relationship between crack width and tensile stress for FRC members. In this model, it was shown that the tensile stress provided by fibers decreases with an increase in crack width; however, the effect of the fiber inclination angle was not considered. In subsequent work by Foster,[3] the evaluation of the tensile stress provided by fibers was made to account for fiber effectiveness as influenced by the random distribution of the fiber angle for fibers having an inclination angle to the crack normal direction less than $\pi/3$. Later, to more reasonably account for the effect of random distribution in the fiber inclination angle, the Variable Engagement Model (VEM)[1] was proposed; it used an effective engagement concept wherein the effectiveness of fibers having an inclination angle less than the critical value increased with an
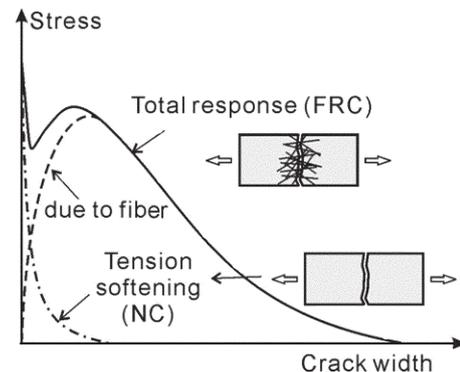
Fig. 1—Tensile behavior of FRC.[1]

increase in the crack width. In this model, the variable fiber embedment lengths were also considered so that variations of the tensile stress in FRC members could be predicted. However, a constant bond stress between the steel fibers and the concrete matrix was assumed; thus, the appropriateness of the model is questionable for end-hooked fiber types. Moreover, fiber slip was assumed to occur only on the side with the shorter length embedment, even though the crack width should equal the sum of the fiber slips from both sides of the crack. The slip from the longer embedded side may not be negligible, particularly when the embedded lengths of the fiber at a crack on either side are relatively similar.

Therefore, for more realistic calculations of the tensile behavior of FRC members, an analysis model is required that can consider the characteristics of fibers whose inclination angles and embedment lengths are randomly distributed. The model should consider the frictional bond behavior and mechanical anchorage effects of fibers and the influence of finite member dimensions.

RESEARCH SIGNIFICANCE

The use of FRC is becoming a more viable and prevalent option in reinforced concrete construction. To analyze and design various FRC structures, a proper evaluation of the tensile response of the material is critical because the tensile behavior of FRC is quite different from that of NC. In this study, an analysis model called the Diverse Embedment Model (DEM) is presented, which considers the pullout characteristics of fibers and their potentially restricted orientation so that the tensile behavior of FRC can

ACI member **Seong-Cheol Lee** is a Postdoctoral Researcher in the Department of Civil Engineering at the University of Toronto, Toronto, ON, Canada. He received his PhD from Seoul National University, Seoul, Korea, in 2007. His research interests include the shear behavior of concrete structures and the analysis of prestressed concrete structures and fiber-reinforced concrete members.

ACI member **Jae-Yeol Cho** is an Assistant Professor in the Department of Civil and Environmental Engineering at Seoul National University, where he also received his PhD. His research interests include nonlinear analysis and optimized design of reinforced and prestressed concrete structures, material modeling, and similitude laws for dynamic testing of concrete structures.

Frank J. Vecchio, FACI, is a Professor in the Department of Civil Engineering at the University of Toronto. He is a member of Joint ACI-ASCE Committees 441, Reinforced Concrete Columns, and 447, Finite Element Analysis of Reinforced Concrete Structures. His research interests include nonlinear analysis and design of reinforced concrete structures, constitutive modeling, performance assessment and forensic investigation, and repair and rehabilitation of structures.

be realistically predicted. The proposed DEM represents a more comprehensive approach than is currently available for the analysis of the structural behavior of reinforced concrete structures with steel fibers.

PULLOUT BEHAVIOR OF SINGLE FIBER

In deriving a tension model for FRC, it is necessary to consider the theoretical pullout behavior of a single fiber under two varying conditions: 1) where only one side of the fiber is embedded in the concrete matrix, whereas the other side is free or fully fixed; and 2) where both sides of the fiber are embedded in the concrete matrix. Because the slip of the longer embedded part of a fiber is not negligible when the embedded lengths on both sides are approximately similar, the pullout behavior of a single fiber embedded on both sides must be considered. The analysis procedure for both straight and end-hooked fibers will be derived to enable the calculation of the fiber stress at a crack, considering the effects of the fiber inclination angle and embedment length. The derived fiber stresses at a crack will be used in the next section for the calculation of the tensile stress provided by fibers.

Pullout behavior of single straight fiber embedded on one side

It can be postulated that, when a crack forms in FRC, the tensile stresses assumed by the fibers bridging the crack are transferred back to the concrete matrix through the bond behavior between the fibers and concrete matrix in the manner shown in Fig. 2. Several researchers[4,5] have derived a corresponding governing equation for the pullout behavior of a single straight fiber with a circular cross section as follows

$$\frac{d^2 s_x}{dx^2} = \tau_{bx} d_f \pi \left(\frac{1}{E_f A_f} + \frac{1}{E_c A_c} \right) \qquad (1)$$

Unlike with common steel reinforcing bar, the fiber length is relatively short compared to its transfer length; thus, the pullout behavior of a straight fiber embedded on one side must be considered to occur in two stages. First, when the slip at the crack is small, the transfer length is less than the embedded length of the fiber; thus, the fiber slips over only part of its embedded length (refer to Fig. 3(a)). In this figure, the slip that may occur before cracking is ignored because it is negligible compared to the slip after cracking. Secondly, when the slip
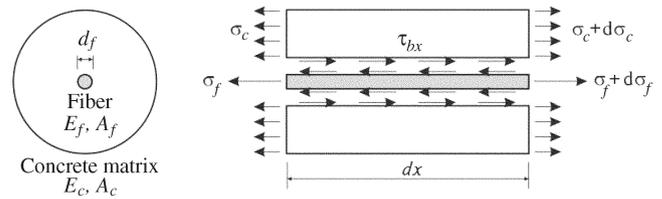
Fig. 2—Free body diagram for infinitesimal element with single straight fiber.
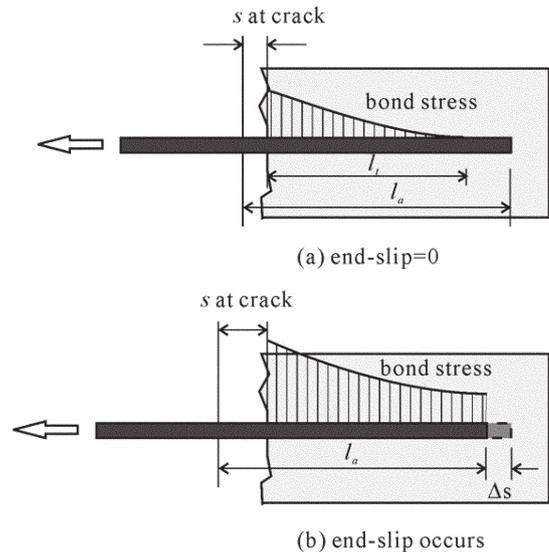
Fig. 3—Pullout behavior of single straight fiber embedded on one side.

at the crack is relatively large, the fiber slip extends over the entire embedded length and slip at the end of the fiber occurs (refer to Fig. 3(b)). For the first stage, the pullout behavior can be mathematically solved, as done for the ordinary reinforced concrete members subjected to uniaxial tension.[6,7] For second-stage behavior, on the other hand, one must consider that the tensile strain of the fiber at the embedded end is different from that of the concrete matrix after end slip has occurred. Here, the fourth-order Runge-Kutta method, which is a numerical method applicable to the solution of second-order differential equations, can be employed to calculate the pullout behavior considering the end-slip effect. With the concrete strain or stress at the fiber end preassumed for the given fiber end slip, the numerical analysis for the bond-stress distribution can be performed using the boundary condition that the concrete stress is zero at the crack.

Figure 4 shows the relationship between the fiber stress and the slip at the crack when the fiber is assumed to be embedded on one side only with half the fiber length. In this analysis example, a bilinear bond stress-slip relationship between the fiber and the concrete matrix was assumed, based on Nammur and Naaman[4] and Lim et al.[8] The tributary area of concrete considered effective was based on a prism diameter of 15 times the fiber diameter suggested by CEB-FIP MC90[9] for ordinary reinforced concrete members. As shown in this figure, the fiber stress at the crack increased linearly up to a peak at which the bond stress reached the full bond strength and then decreased linearly because of the ensuing reduction in the embedded length of the fiber. Figure 5, which shows the corresponding variation of the
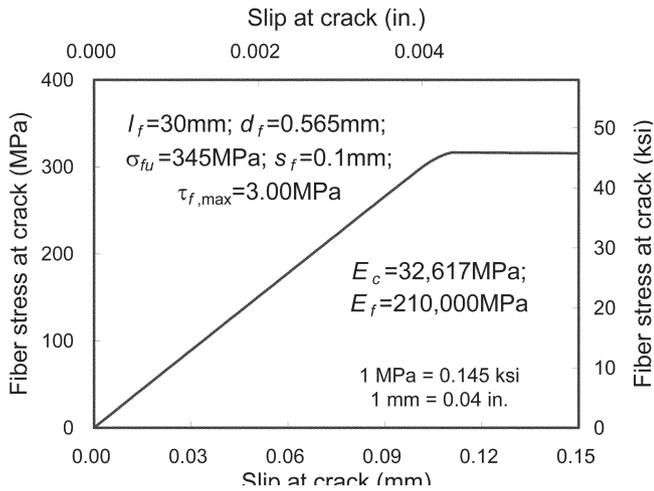
Fig. 4—Fiber stress at crack with $l_a = 0.5l_f$ for straight fiber.
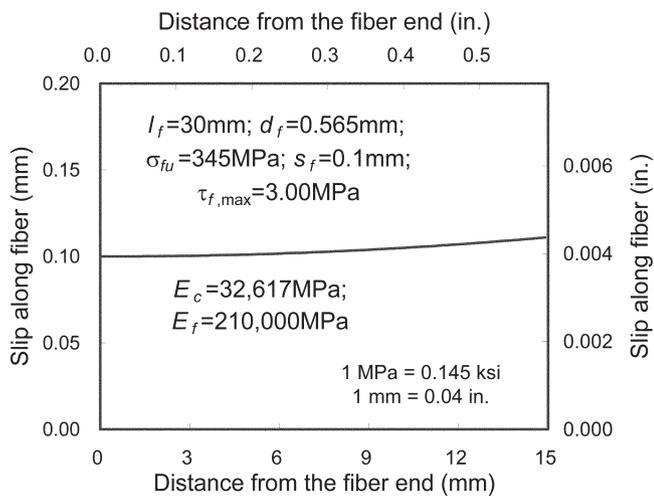
Fig. 5—Variation of slip along straight fiber when end slip is 0.1 mm (0.004 in.).
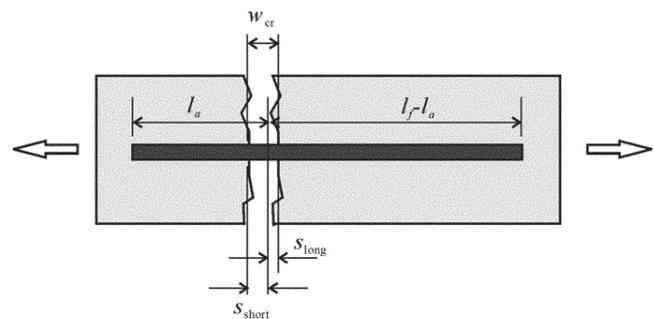
Fig. 6—Pullout behavior of fiber embedded on both sides.

slip along the fiber for this case, indicates that the variation is negligible. Therefore, it can be assumed that the slip can be considered as constant along the fiber, and that the elongation of the fiber can be neglected. In other words, for simplicity, the pullout behavior of a single straight fiber can be considered as the rigid body translation, which means that displacement due to elastic strains in the fibers can be neglected, as assumed in the VEM.[1]

Pullout behavior of single straight fiber embedded on both sides

Figure 6 represents the pullout conditions of a fiber embedded on both sides when the fiber is perpendicular to the crack surface. The crack width equals the sum of slips from both sides of the cracked concrete. Note that the slip of the shorter embedded part is larger than that of the longer embedded part with the assumption of the rigid body translation for the pullout behavior of a single straight fiber; this is because the bond stress between the fiber and the concrete matrix for the shorter part must be larger to satisfy force equilibrium of the fiber at the crack. With the assumption of rigid body translation of the fiber and a bilinear bond stress-slip relationship between the fiber and the concrete matrix, the following force equilibrium equation can be derived when the slip for the shorter embedded part of the fiber is less than slip s_f

$$\pi d_f \left(l_a - s_{short}\right) K_f s_{short} = \pi d_f \left(l_f - l_a - s_{long}\right) K_f s_{long}$$

$$\text{for } s_{short} \le s_f \tag{2a}$$

where s_f is the slip corresponding to the full bond strength; and K_f is the bond modulus.

When the slip for the shorter embedded part is larger than s_f, the bond behavior of the longer embedded part can be considered as an unloading mechanism on the bond stress-slip relationship while the bond stress of the shorter embedded part reaches the bond strength. Hence, the equilibrium condition for this case can be formulated as follows

$$\pi d_f \left(l_a - s_{short}\right) \tau_{f,max} = \pi d_f \left(l_f - l_a - s_{long}\right) K_f s_{long}$$

$$\text{for } s_{short} > s_f \tag{2b}$$

From Eq. (2(a)) and (2(b)) and $\tau_{f,max} = s_f K_f$, the slip for the longer embedded part can be calculated as a function of the given s_{short} from the following equations

$$s_{long} = \frac{l_f - l_a - \sqrt{\left(l_f - l_a\right)^2 - 4\left(l_a - s_{short}\right)s_{short}}}{2}$$

$$\text{for } s_{short} \le s_f \tag{3a}$$

$$s_{long} = \frac{l_f - l_a - \sqrt{\left(l_f - l_a\right)^2 - 4\left(l_a - s_{short}\right)s_f}}{2}$$

$$\text{for } s_{short} > s_f \tag{3b}$$

The tensile stress of the fiber at the crack can then be calculated using the following relation

$$\sigma_{f,cr} = \frac{4\tau_{short}\left(l_a - s_{short}\right)}{d_f} = \frac{4K_f s_{long}\left(l_f - l_a - s_{long}\right)}{d_f} \ge 0 \tag{4}$$

Figure 7 describes the variation of the fiber stress at a crack determined accordingly, displayed as a function of the crack width, which is the sum of the slips at the crack from both sides of the fiber and the shorter embedment length. It is evident in this figure that as the fiber embedded lengths to each side approach one-half the fiber length, the crack width for the peak fiber stress at the crack increases to $2s_f$. Also, the fiber stress at the crack increases to that calculated
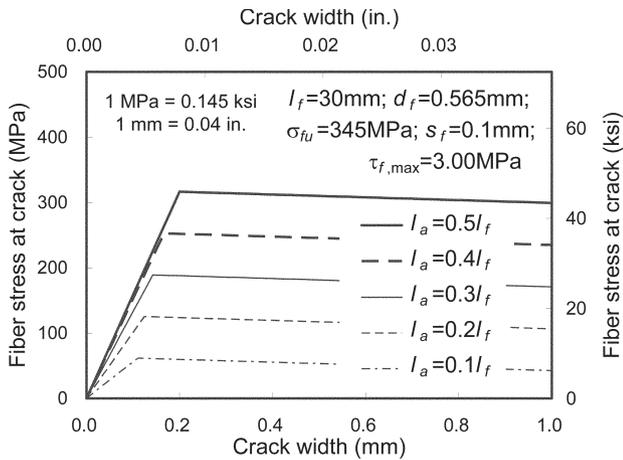
Fig. 7—Fiber stress at crack: crack width response.
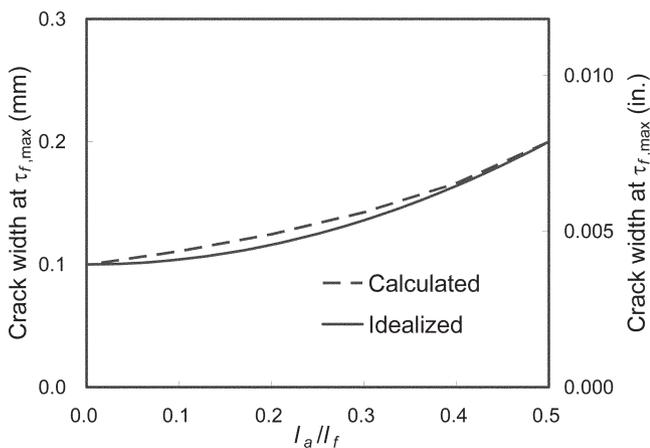
Fig. 8—Crack width at maximum pullout stress.

using Eq. (4) with $s_{short} = s_{long} = s_f$ for the pullout strength of a fiber having an embedded length equal to one-half the fiber length. Therefore, in comparing Fig. 4 and Fig. 7, the crack width at the maximum fiber stress at a crack varies from s_f to $2s_f$ for fibers in which both sides are embedded according to the embedded length, whereas the slip at the peak stress for fibers in which only one side is embedded is fixed at s_f, regardless of the embedded length of the fiber.

Fibers normal to crack surface—In calculations of the tensile stress in FRC, it is more convenient to use crack width as the defining parameter rather than the slip at the crack because the crack width can be directly calculated by multiplying the average tensile strain and the crack spacing. Figure 8 shows the relationship between the nondimensional shorter embedment length ratio l_a/l_f and crack width at the maximum pullout stress. As evident in this figure, the crack width at the maximum pullout stress of the fiber at the crack can be idealized with respect to the ratio of the shorter embedded length to the fiber length.

$$w_{p0} = s_f \left[1 + 4 \left(\frac{l_a}{l_f} \right)^2 \right] \quad (5)$$

Because the relationship between the fiber stress at the crack and the crack width can be considered to be bilinear, the bond stress for the shorter embedded part of the fiber, which is used for the calculation of the tensile stress, can be calculated for the given crack width.

$$\tau_{short} = \frac{w_{cr}}{w_{p0}} \tau_{f,max} \quad \text{for} \quad w_{cr} \leq w_{p0} \quad (6a)$$

$$\tau_{short} = \tau_{f,max} \quad \text{for} \quad w_{cr} > w_{p0} \quad (6b)$$

Fibers inclined to crack surface—In addition to the random distribution of fiber embedment length, the effect of fiber orientation should also be considered when evaluating the tensile stress developed by fibers. To investigate the effect of fiber orientation, Banthia and Trottier[10] conducted pullout tests on crimped single fibers, which can be considered similar to straight fibers embedded with various fiber inclination angles. Figure 9(a) shows how the frictional

(a)

(b)
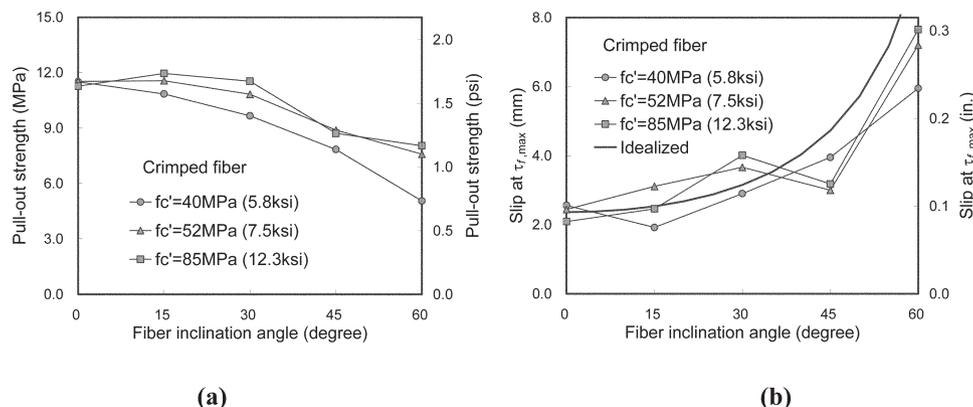
Fig. 9—Effect of fiber inclination angle on behavior of crimped fiber from tests by Banthia and Trottier[10]: (a) frictional pullout strength; and (b) slip at frictional pullout strength.
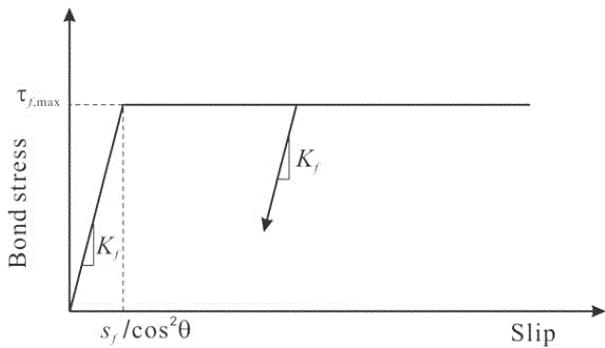
Fig. 10—Bond slip-stress relationship due to friction for inclined fiber from Nammur and Naaman.[4]
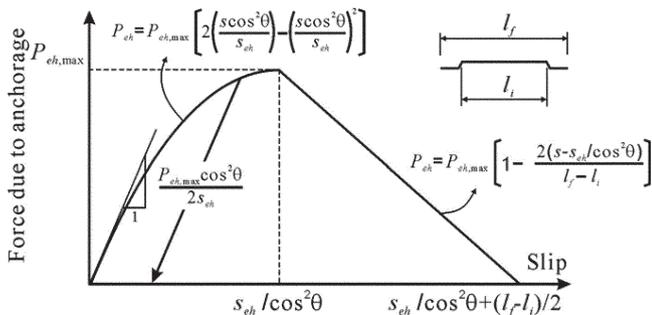
Fig. 11—Idealized relationship between slip and pullout force due to mechanical anchorage of end-hooked fiber.

pullout strength of the fiber is affected by the fiber inclination angle, defined as the difference between the fiber orientation and normal to the crack surface. As shown in this figure, the frictional pullout strength for the crimped steel fiber is only slightly affected by the fiber inclination angle for angles less than 30 degrees, whereas it decreases with an increasing fiber inclination angle for angles larger than 30 degrees. From experimental tests with steel fibers, Ouyang et al.[11] reported that the pullout strength of inclined fibers was generally greater than that of aligned fibers, whereas Lee and Foster[12] reported that the pullout strength of a straight fiber decreased with an increase in the fiber inclination angle. Given these contradictions between findings by previous researchers, the effect of the fiber inclination angle on the pullout strength is not yet clear. For analytical simplicity in this study, the bond strength is assumed to be constant, regardless of the variation of the fiber inclination angle.

Unlike the effect of the fiber inclination angle on the bond strength, it was determined by Banthia and Trottier[10] that the slip at the peak pullout load increases with an increase in the fiber inclination. Through comparisons with the experimental results, as shown in Fig. 9(b), the variation of the slip at the maximum pullout load $s_{f\theta}$ can be idealized according to Eq. (7) (refer also to Fig. 10).

$$s_{f\theta} = s_f/\cos^2\theta \qquad (7)$$

Using Eq. (6(a)) and (6(b)) and Fig. 10, the bond stress for the shorter embedded part of a fiber with inclination angle θ can be calculated for the given crack width

$$\tau_{short} = \frac{w_{cr}}{w_{p\theta}}\tau_{f,max} \quad \text{for} \quad w_{cr} \leq w_{p\theta} \qquad (8a)$$

$$\tau_{short} = \tau_{f,max} \quad \text{for} \quad w_{cr} > w_{p\theta} \qquad (8b)$$

where $w_{p\theta} = s_f[1 + 4(l_a/l_f)^2]/\cos^2\theta$.

With the compatibility condition that $w_{cr} = s_{long} + s_{short}$ and using Eq. (2), the slip for the shorter embedded part can thus be calculated for the given crack width as follows

$$s_{short} = \frac{(l_f - l_a)w_{cr} - w_{cr}^2}{l_f - 2w_{cr}} \quad \text{for} \quad w_{cr} \leq w_{p\theta} \qquad (9a)$$

$$s_{short} = \frac{-B + \sqrt{B^2 - 4C}}{2} \quad \text{for} \quad w_{cr} > w_{p\theta} \qquad (9b)$$

where $B = l_f - l_a - 2w_{cr} - s_{f\theta}$; and $C = l_a s_{f\theta} - (l_f - l_a - w_{cr})w_{cr}$.

Because the fiber stress at the crack reaches its peak value when the crack width is $w_{p\theta}$, the maximum stress that the fiber experiences can be calculated from Eq. (4) and (9(a)) as follows

$$\sigma_{f,cr,exp} = \frac{4w_{cr}}{w_{p\theta}}\left[l_a - \frac{(l_f - l_a)w_{cr} - w_{cr}^2}{l_f - 2w_{cr}}\right]\frac{\tau_{f,max}}{d_f} \qquad (10)$$

where w_{cr} is not larger than $w_{p\theta}$. If the calculated maximum experienced stress is larger than the fiber tensile strength, it can be concluded that the fiber has already ruptured.

Pullout behavior of single end-hooked fiber embedded on both sides

Unlike the anchorage of a straight steel fiber, which can be characterized by frictional bond behavior alone, an end-hooked steel fiber also benefits from mechanical anchorage provided by the end hook. Sujivorakul et al.[13] reported that end-hooked fibers exhibited much larger pullout forces than straight fibers, and that the difference in the pullout load between the two fiber types came from the mechanical anchorage of the end hooks. In this study, the tensile force provided by the mechanical anchorage is idealized with a parabolic and linear relationship for the pre- and post-peak behaviors, respectively, as shown in Fig. 11. For the descending regime, after the slip amount exceeds the length of the end hook, it can be assumed that the tensile force due to the mechanical anchorage becomes zero because of the deterioration of the concrete matrix near the mechanical end hook and the straightening of the hook.

The effect of the inclination angle on the behavior of end-hooked fibers will be modeled according to the trends portrayed in Fig. 12. It will be assumed that the slip at peak bond stress (relating to the friction mechanism) and the slip at peak tensile force (relating to the mechanical anchorage mechanism) both increase with an increasing angle in a manner similar to the frictional bond slip observed in straight fibers, as influenced by the fiber inclination angle. After the shorter embedded part of a fiber reaches its pullout strength, the shorter embedded part follows the post-peak behavior for the mechanical anchorage effect, whereas the
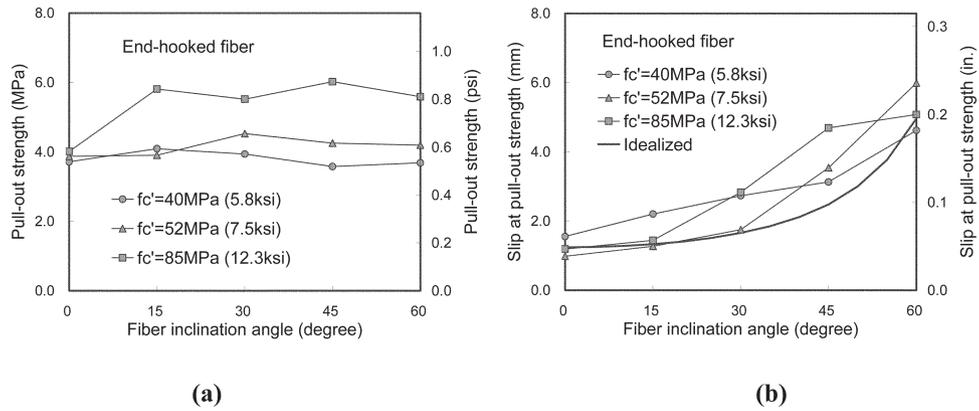
Fig. 12—Effect of inclination angle on behavior of end-hooked fiber from tests by Banthia and Trottier[10]: (a) pullout strength; and (b) slip at pullout strength.

longer embedded part undergoes partial unloading for both the frictional bond and the mechanical anchorage stresses.

To calculate the stress at the crack in an end-hooked steel fiber, three possible cases should be considered with respect to the force equilibrium at a crack: 1) the end hook in the shorter embedded part of the fiber remains embedded; 2) the end hook is pulled out; and 3) the end hook in the shorter embedded part of the fiber was not originally fully embedded.

The force equilibrium condition in Case 1 can be described as follows

$$\pi d_f \left(l_a - s_{short}\right) \tau_{short} + P_{eh,short}$$
$$= \pi d_f \left(l_f - l_a - s_{long}\right) \tau_{long} + P_{eh,long} \qquad (11)$$
$$\text{for } l_a - s_{short} > \left(l_f - l_i\right)/2$$

The slips, bond stresses, and tensile forces at the mechanical anchorages can be calculated for a given crack width through an iterative procedure for s_{short} using the previous equation in which the frictional bond stresses and the mechanical anchorage forces can be determined from Fig. 11 and 12. Thus, the fiber stress at a crack is calculated from the sum of the stresses due to the mechanical anchorage and the frictional bond stress along the fiber as follows

$$\sigma_{f,cr} = \frac{4\tau_{short}\left(l_a - s_{short}\right)}{d_f} + \frac{4P_{eh,short}}{\pi d_f^2} \qquad (12)$$

To check whether fiber rupture has occurred, when the slip in the shorter embedded side is larger than the slip causing the maximum pullout force, the maximum experienced fiber stress at a crack can be calculated as

$$\sigma_{f,cr,exp} = \frac{4P_{eh,max}}{\pi d_f^2} + \frac{4\tau_f\left(l_a - \dfrac{s_{eh}}{\cos^2\theta}\right)}{d_f} \qquad (13)$$

$$\text{for } s_{short} > s_{eh}/\cos^2\theta$$

where $P_{eh,max}$ can be found from the frictional bond strength of a straight fiber $\tau_{f,max}$; and the pullout strength of an end-hooked fiber $\tau_{eh,max}$ can be expressed as follows

$$P_{eh,max} = \left(\tau_{eh,max} - \tau_{f,max}\right)\left(\frac{l_f}{2} - s_{eh}\right)\pi d_f \qquad (14)$$

When s_{short} is less than $s_{eh}/\cos^2\theta$, the current fiber stress at the crack is the maximum experienced value. If the maximum experienced stress is larger than the fiber strength, the fiber has already ruptured.

With Case 2, when l_a is between $(l_f - l_i)/2 + s_{short}$ and $(l_f - l_i)/2$, it can be assumed that the pullout of the mechanical anchorage causes deterioration of the concrete matrix near it. Therefore, the bond stress along the still embedded part of the fiber can be neglected. For Case 3, because the combined anchorage resistance of the longer embedded part of the fiber is much greater than that of the shorter part, it can be assumed that the slip from the shorter embedded side is the dominant contributor to the crack width. Hence, Case 3 can be simplified by assuming that the fiber stress at a crack can be calculated from the pullout behavior of a straight fiber that is embedded on only one side.

CONSIDERATION OF MEMBER DIMENSION AND FIBER EMBEDDED LENGTH

Generally, it can be assumed that the fiber inclination angle and the fiber embedment length, with respect to cracks in the concrete matrix, are randomly distributed. Using the formulations for individual fiber stress at a crack developed in the previous section, the average fiber stress in randomly distributed fibers at a crack can now be derived. Finite member dimensions may affect the fiber orientation, however; this influence will now also be taken into account.

General fiber orientation in three-dimensional (3-D) infinite member

Steel fibers randomly oriented in a 3-D infinite element can be illustrated with a sphere, as shown in Fig. 13.[1,14,15] Because the probability density for the fiber inclination angle can be expressed with a sine function, the fiber stress at a crack, averaged over the full range of fiber inclination angles, can be calculated with the following equation.
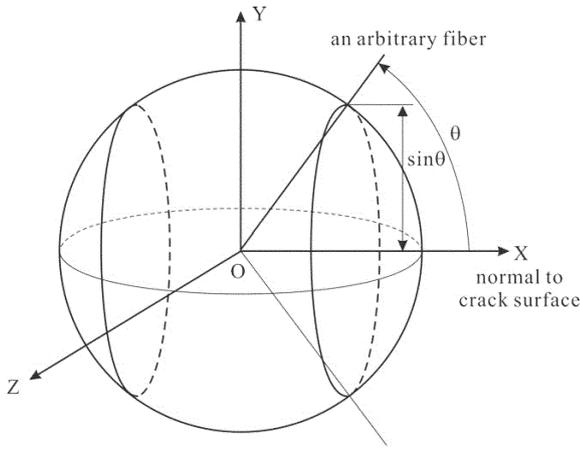
Fig. 13—Probability of fiber inclination angle using sphere representation.[1,14,15]
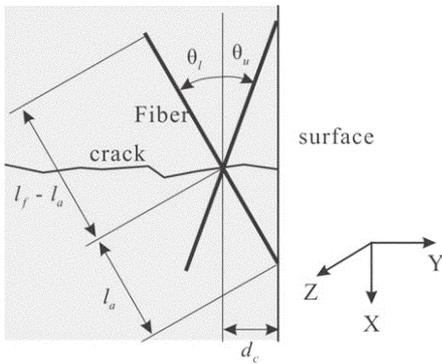
Fig. 14—Effect of boundary surface on fiber inclination angle.

$$\sigma_{f,cr,\theta} = \int_0^{\pi/2} \sigma_{f,cr}\left(l_a,\theta\right)\sin\theta \, d\theta \qquad (15)$$

Fiber orientation in two-dimensional (2-D) member

In general, because fresh concrete is placed in forms, fiber orientation will be influenced by the dimensions of the member and the finishing of exposed surfaces. Assuming that the crack surface is perpendicular to the boundary surface, as in uniaxial tensile specimens with a rectangular cross section, the possible fiber orientation conditions in members whose thickness is larger than double the fiber length can be divided into three cases: 1) the fiber orientation is affected by both long and short parts of the fiber; 2) the fiber orientation is affected by only the longer part; and 3) the fiber orientation is not affected. From the geometrical conditions shown in Fig. 14, the possible angle of fiber orientation in 2-D members can be calculated by the following.

$$-\theta_l\left(l_a\right) = -\sin^{-1}\left(\min\left(1,\frac{d_c}{l_a}\right)\right)$$
$$\leq \theta \leq \sin^{-1}\left(\min\left(1,\frac{d_c}{l_f - l_a}\right)\right) = \theta_u\left(l_a\right) \qquad (16)$$

In members with a thickness less than twice the fiber length, the effect of both boundary surfaces on the fiber

orientation can be simply considered in the same manner using the previous equation.

Because the probability density for the fiber inclination angle θ is $\sin\theta$ in an infinite member (refer to Fig. 13), and the total possible area for the fiber inclination angle is $2\pi(\sin\theta_u + \sin\theta_l)$, as shown in Fig. 15(a), the fiber stress at a crack considering the effect of member thickness, which is averaged through the variation of the fiber inclination angle, can be calculated as follows

$$\sigma_{f,cr,\theta}\left(l_a\right)$$

$$= \frac{2\int_0^{\pi/2} \sigma_{f,cr}\left(l_a,\theta\right)\left(\theta_{uc}\left(l_a,\theta\right) + \theta_{lc}\left(l_a,\theta\right)\right)\sin\theta \, d\theta}{\pi\left(\sin\theta_u\left(l_a\right) + \sin\theta_l\left(l_a\right)\right)} \qquad (17)$$

where $\theta_{uc} = \sin^{-1}(\min(1,\sin\theta_u/\sin\theta))$ and $\theta_{lc} = \sin^{-1}(\min(1,\sin\theta_l/\sin\theta))$, respectively, as illustrated in Fig. 15(b).

Fiber orientation in 3-D finite member

The procedure for determining the fiber inclination angle in a 2-D member, presented previously, can be expanded to 3-D members. Consider members with a rectangular cross section subjected to uniaxial tension, where it can be assumed that a crack surface is always perpendicular to the boundary surfaces, as in dog-bone specimens commonly tested to investigate the uniaxial tensile behavior of FRC. Here, the possible surface area for the fiber inclination angle on a sphere having a radius of unit length, as shown in Fig. 16, can be calculated as follows

$$A_\theta = 2\int_0^{\pi/2}\left(\begin{array}{c}\theta_{uuc}\left(l_a,\theta\right) + \theta_{llc}\left(l_a,\theta\right) \\ + \theta_{ulc}\left(l_a,\theta\right) + \theta_{luc}\left(l_a,\theta\right)\end{array}\right)\sin\theta \, d\theta \qquad (18)$$

where $\theta_{uuc} = \max(0,\theta_{ucy} - 0.5\pi + \theta_{ucz})$; $\theta_{ulc} = \max(0,\theta_{ucy} - 0.5\pi + \theta_{lcz})$; $\theta_{luc} = \max(0,\theta_{lcy} - 0.5\pi + \theta_{ucz})$; $\theta_{llc} = \max(0,\theta_{lcy} - 0.5\pi + \theta_{lcz})$ with $\theta_{ucy} = \sin^{-1}(\min(1,\sin\theta_{uy}/\sin\theta))$; $\theta_{lcy} = \sin^{-1}(\min(1,\sin\theta_{ly}/\sin\theta))$; $\theta_{ucz} = \sin^{-1}(\min(1,\sin\theta_{uz}/\sin\theta))$; and $\theta_{lcz} = \sin^{-1}(\min(1,\sin\theta_{lz}/\sin\theta))$.

In the previous equation, θ_{uy}, θ_{ly}, θ_{uz}, and θ_{lz} are calculated from the following

$$-\theta_{ly}\left(l_a\right) = -\sin^{-1}\left(\min\left(1,\frac{d_{cy}}{l_a}\right)\right) \leq \theta_y$$
$$\leq \sin^{-1}\left(\min\left(1,\frac{d_{cy}}{l_f - l_a}\right)\right) = \theta_{uy}\left(l_a\right) \qquad (19a)$$

$$-\theta_{lz}\left(l_a\right) = -\sin^{-1}\left(\min\left(1,\frac{d_{cz}}{l_a}\right)\right) \leq \theta_z$$
$$\leq \sin^{-1}\left(\min\left(1,\frac{d_{cz}}{l_f - l_a}\right)\right) = \theta_{uz}\left(l_a\right) \qquad (19b)$$

The area considering the fiber stress at a crack can also be calculated according to the following integration.
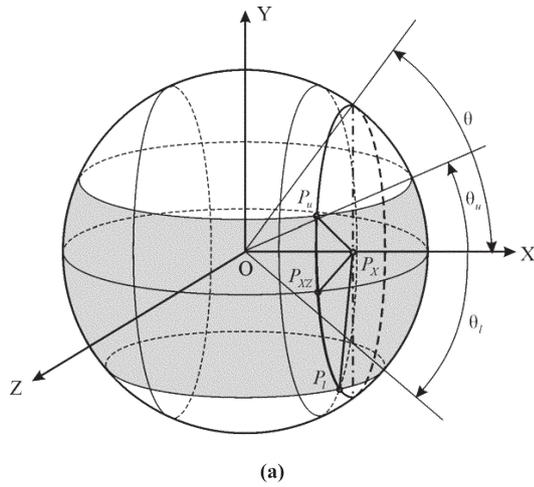
(a)
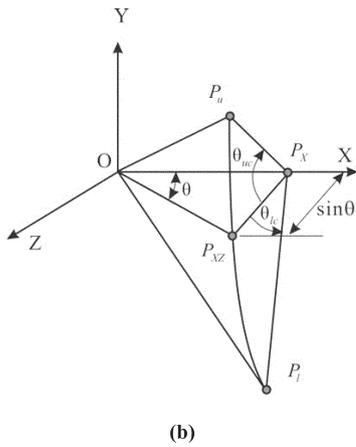
(b)

Fig. 15—Fiber inclination angle in 2-D: (a) surface area on sphere representing fiber angle; and (b) fiber inclination angle contribution to tension.

$$A_\sigma = 2\int_0^{\pi/2} \sigma_{f,cr}(l_a,\theta)\left(\begin{array}{c}\theta_{uuc}(l_a,\theta) + \theta_{llc}(l_a,\theta) \\ + \theta_{ulc}(l_a,\theta) + \theta_{luc}(l_a,\theta)\end{array}\right)\sin\theta\, d\theta \quad (20)$$

Thus, using Eq. (18) and (20), the fiber stress at a crack considering the random distribution of the fiber inclination angle in a 3-D finite member can be calculated as

$$\sigma_{f,cr,\theta}(l_a) = \frac{A_\sigma}{A_\theta}$$

$$= \frac{\int_0^{\pi/2} \sigma_{f,cr}(l_a,\theta)\left(\begin{array}{c}\theta_{uuc}(l_a,\theta) + \theta_{llc}(l_a,\theta) \\ + \theta_{ulc}(l_a,\theta) + \theta_{luc}(l_a,\theta)\end{array}\right)\sin\theta\, d\theta}{\int_0^{\pi/2}\left(\begin{array}{c}\theta_{uuc}(l_a,\theta) + \theta_{llc}(l_a,\theta) \\ + \theta_{ulc}(l_a,\theta) + \theta_{luc}(l_a,\theta)\end{array}\right)\sin\theta\, d\theta} \quad (21)$$

Average fiber stress at crack considering fiber orientation and fiber embedment length

In addition to the random orientation of fibers, the randomness of the fiber embedment length should also be considered in the calculation of the average fiber stress at a crack. With the assumption that the probability for the fiber

(a)

the angle contributing on tensile behavior

the angle contributing on tensile behavior
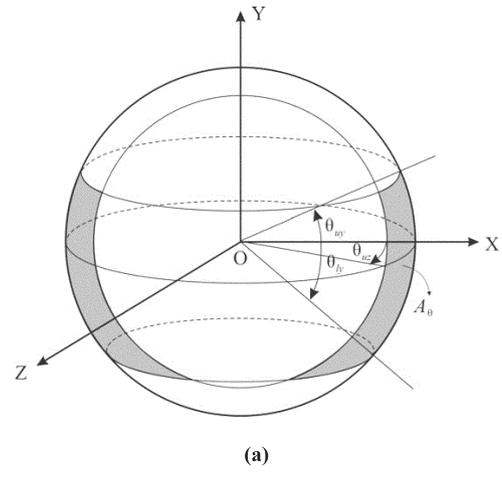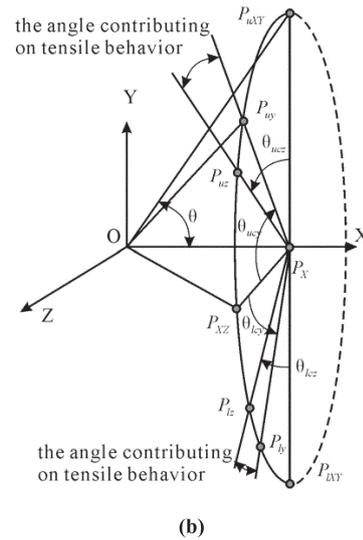
(b)

Fig. 16—Fiber inclination angle in 3-D: (a) surface area on sphere representing fiber angle; and (b) fiber inclination angle contribution to tension.

embedment length at initial cracking is uniform, the average fiber stress at a crack considering the randomly distributed fiber inclination angles and fiber embedment lengths can be calculated from Eq. (15), (17), and (21) as follows.

$$\sigma_{f,cr,avg} = \frac{1}{l_f/2}\int_0^{l_f/2}\sigma_{f,cr,\theta}(l_a)\, dl_a \quad (22)$$

DERIVATION OF FIBER ORIENTATION FACTOR CONSIDERING MEMBER DIMENSION

To define the tensile stress on a crack surface of unit area, the number of fibers crossing the surface should be known; this number is commonly expressed by employing a fiber orientation factor α_f as follows

$$N_f = \alpha_f \frac{V_f}{A_f} \quad (23)$$

It is well known that the fiber orientation factor can be affected by the member size because fiber orientations can be influenced by the boundary surface. Based on work by

Romualdi and Mandel,[16] Soroushian and Lee[17,18] presented a formulation for the average fiber orientation factor considering the effect of member size. In their work, a constant probability function was used for the variation of the angles between the fiber and two perpendicular axes that are parallel to the crack surface, respectively. On the other hand, Aveston and Kelly[14] derived the fiber orientation factor with the assumption that the probability density for the fiber inclination angle should be a sine function in an infinite element. Several decades later, Li et al.[15] and Stroeven[19] also argued that the probability density for the fiber inclination angle should be variable, as Aveston and Kelly[14] had suggested. Moreover, experimental results obtained by Gettu et al.[20] indicated that the fiber orientation factor decreased from the boundary surface to the center of the cross section. This means that the variation of the fiber orientation factor along the cross section in 2-D or 3-D members should be taken into account to more reasonably evaluate the tensile stress provided by the fibers. Thus, in this section, a fiber orientation factor, which is variable along the section, will be derived considering the effect of member dimension following the approach of Aveston and Kelly.[14]

Because the number of fibers crossing the unit area of the crack surface is $N\cos\theta$ for fibers aligned with an inclination angle θ, Aveston and Kelly[14] derived the fiber orientation factor in an infinite element, as given by the following equation.

$$\alpha_f = \int_0^{\pi/2} \cos\theta \sin\theta d\theta = 0.5 \qquad (24a)$$

In the previous equation, $\sin\theta$ refers to the probability density, as illustrated in Fig. 13.

If the member size is relatively small compared with the fiber length, it should be considered that the fiber inclination angle will be significantly affected by the boundary surfaces. In the same manner as the procedure for calculating the average fiber stress at a crack (refer to Fig. 15 and 16), the fiber orientation factor considering the effect of member thickness in a 2-D member or the size of the rectangular section in a 3-D member can be expressed by the following equations, respectively.

$$\alpha_{f,2D} = \frac{2}{l_f} \int_0^{l_f/2} \frac{2\int_0^{\pi/2} \cos\theta \left(\begin{array}{c} \theta_{uc}\left(l_a,\theta\right) \\ + \theta_{lc}\left(l_a,\theta\right) \end{array} \right) \sin\theta d\theta}{\pi\left(\sin\theta_u\left(l_a\right) + \sin\theta_l\left(l_a\right)\right)} dl_a \qquad (24b)$$

$$\alpha_{f,3D} = \frac{2}{l_f} \int_0^{l_f/2} \frac{\int_0^{\pi/2} \cos\theta \left(\begin{array}{c} \theta_{uuc}\left(l_a,\theta\right) + \theta_{llc}\left(l_a,\theta\right) \\ + \theta_{ulc}\left(l_a,\theta\right) + \theta_{luc}\left(l_a,\theta\right) \end{array} \right) \sin\theta d\theta}{\int_0^{\pi/2} \left(\begin{array}{c} \theta_{uuc}\left(l_a,\theta\right) + \theta_{llc}\left(l_a,\theta\right) \\ + \theta_{ulc}\left(l_a,\theta\right) + \theta_{luc}\left(l_a,\theta\right) \end{array} \right) \sin\theta d\theta} dl_a \quad (24c)$$

TENSILE STRESS CAPACITY PROVIDED BY FIBERS

The tensile stress capacity provided by fibers in a 3-D infinite member can easily be calculated from Eq. (23) and (24(a)), producing the following equation, because the fiber orientation factor is not affected by the variation of the crack width.

$$f_f = \alpha_f V_f \sigma_{f,cr,avg} \qquad (25a)$$

In a member with a rectangular cross section, the tensile stress provided by the fibers averaged through the cross section can be calculated as follows.

$$f_f = \frac{1}{A_c} \int_{A_c} \alpha_{f,3D}\left(y,z\right) V_f \sigma_{f,cr,avg}\left(y,z\right) dA_c \qquad (25b)$$

The tensile stress provided by fibers from the previous equation can be very useful for the realistic analysis of the uniaxial tensile behavior of FRC members with a rectangular cross section whose size is relatively small compared to the fiber length. Equation (25(b)) can be used for a 2-D element for which the thickness effect is only considered. The tensile stress of FRC can then be calculated from the sum of the tensile stresses provided by fibers and tension softening of the concrete matrix.

CONCLUSIONS

In this paper, the DEM was presented as an analysis procedure for evaluating the average tensile stress developed in fibers across a crack in FRC members subjected to tension. To derive the tensile stress of a single fiber at a crack, equilibrium and compatibility conditions were considered in the analysis of the pullout behavior of a single fiber embedded on both sides. The pullout characteristics associated with the two main anchorage mechanisms—frictional bond behavior and mechanical end-hook anchorage—were explicitly considered in the formulation. From the individual fiber stresses at a crack, the average tensile stress of fibers at a crack was derived by incorporating the randomness of fiber inclination angles and fiber embedment lengths. Because the distribution of fiber inclination angles can be affected by the boundary surfaces in finite-sized members, the probabilities for the fiber inclination angle were derived for three cases: 1) 3-D infinite elements; 2) 2-D finite thickness elements; and 3) 3-D finite-sized elements with rectangular sections. Fiber orientation factors considering member dimensions were derived for these element types. Consequently, the average tensile stress carried by fibers can be calculated from the average tensile stress of fibers at a crack, the fiber orientation factor, and the fiber volumetric ratio. The total response of SFRC members can thus be calculated from the sum of the fiber tensile stresses and the concrete tension softening stresses. The proposed model can be useful for the realistic analysis of FRC elements subjected to tension. The details of verification studies and related discussions for the proposed analysis model are presented in an accompanying paper.[21]

NOTATION

A_c, A_f = cross-sectional areas of concrete matrix and fiber, respectively
A_θ = area of surface describing possible fiber inclination angle on sphere
A_σ = area of surface describing possible fiber inclination angle on sphere considering variation of fiber stress at crack
d_c = distance from boundary surface in 2-D element
d_{cy}, d_{cz} = distances from boundary surface to y- and z-axis in 3-D element, respectively

d_f	=	fiber diameter
E_c, E_f	=	elastic modulus of concrete matrix and fiber, respectively
f'_c	=	concrete compressive strength
f_f	=	tensile stress due to fibers for given crack width
l_a	=	fiber embedment length on shorter side
l_f	=	fiber length
l_i	=	distance between mechanical anchorages for end-hooked fiber
K_f	=	bond modulus, which is slope for elastic behavior in bond stress-slip relationship for fiber, of which inclination angle is 0 degrees
N_f	=	number of fibers crossing crack surface with unit area
$P_{eh,long}, P_{eh,short}$	=	tensile forces due to mechanical anchorage of longer and shorter embedded part of end-hooked fiber, respectively
$P_{eh,max}$	=	maximum tensile force due to mechanical anchorage of end-hooked fiber
s	=	slip of fiber
s_{eh}	=	slip at $P_{eh,max}$
s_f	=	slip at frictional bond strength for fiber with inclination angle of 0 degrees
$s_{f\theta}$	=	slip at frictional bond strength for fiber with inclination angle of θ
s_{long}	=	slip at crack for longer embedded part of fiber
s_{short}	=	slip at crack for shorter embedded part of fiber
s_x	=	slip between fiber and matrix at location x
V_f	=	fiber volumetric ratio
w_{cr}	=	crack width
w_{p0}	=	crack width at bond strength for fiber with inclination angle of 0 degrees
$w_{p\theta}$	=	crack width at bond strength for fiber with inclination angle of θ
x	=	distance from a crack
y, z	=	locations to axes that are parallel to crack surface in cross section
α_f	=	fiber orientation factor
$\alpha_{f,2D}$	=	local fiber orientation factor considering member thickness in 2-D element
$\alpha_{f,3D}$	=	local fiber orientation factor considering member thickness and width in 3-D element
θ	=	fiber inclination angle from axis that is perpendicular to crack surface
θ_l, θ_u	=	lower and upper limits for fiber inclination angle considering effect of boundary surface in 2-D element as presented in Fig. 15(a), respectively
$\theta_{ly}, \theta_{uy}, \theta_{lz}, \theta_{uz}$	=	lower and upper limits for fiber angle from XZ or YZ planes considering effect of boundary surface in 3-D element as presented in Fig. 16(a), respectively
$\sigma_{f,cr}$	=	fiber stress at crack with given fiber inclination angle and embedment length
$\sigma_{f,cr,avg}$	=	average fiber stress at crack considering random distributions of fiber inclination angle and embedment length
$\sigma_{f,cr,exp}$	=	maximum experienced fiber stress at crack
$\sigma_{f,cr,\theta}$	=	fiber stress at crack averaged through variation of θ for given length l_a
σ_{fu}	=	ultimate tensile strength of fiber
τ_{bx}	=	bond stress between fiber and matrix at location x
$\tau_{f,max}$	=	frictional pullout strength for end-hooked fiber or straight fiber
$\tau_{eh,max}$	=	pullout strength of end-hooked fiber
$\tau_{long}, \tau_{short}$	=	frictional bond stress for longer or shorter embedded part of fiber, respectively

REFERENCES

1. Voo, J. Y. L., and Foster, S. J., "Variable Engagement Model for Fibre Reinforced Concrete in Tension," *Uniciv Report No. R-420*, School of Civil and Environmental Engineering, The University of New South Wales, Sydney, Australia, June 2003, 86 pp.

2. Marti, P.; Pfyl, T.; Sigrist, V.; and Ulaga, T., "Harmonized Test Procedures for Steel Fiber-Reinforced Concrete," *ACI Materials Journal*, V. 96, No. 6, Nov.-Dec. 1999, pp. 676-686.

3. Foster, S. J., "On Behavior of High-Strength Concrete Columns: Cover Spalling, Steel Fibers, and Ductility," *ACI Structural Journal*, V. 98, No. 4, July-Aug. 2001, pp. 583-589.

4. Nammur Jr., G., and Naaman, A. E., "Bond Stress Model for Fiber Reinforced Concrete Based on Bond Stress-Slip Relationship," *ACI Materials Journal*, V. 86, No. 1, Jan.-Feb. 1989, pp. 45-57.

5. Naaman, A. E.; Namur, G. G.; Alwan, J. M.; and Najm, H. S., "Fiber Pullout and Bond Slip I: Analytical Study," *Journal of Structural Engineering*, ASCE, V. 117, No. 9, Sept. 1991, pp. 2769-2790.

6. Balázs, G. L., "Cracking Analysis Based on Slip and Bond Stresses," *ACI Materials Journal*, V. 90, No. 4, July-Aug. 1993, pp. 320-348.

7. Oh, B. H., and Kim, S. H., "Advanced Crack Width Analysis of Reinforced Concrete Beams under Repeated Loads," *Journal of Structural Engineering*, ASCE, V. 133, No. 3, Mar. 2007, pp. 411-420.

8. Lim, T. Y.; Paramasivam, P.; and Lee, S. L., "Analytical Model for Tensile Behavior of Steel-Fiber Concrete," *ACI Materials Journal*, V. 84, No. 4, July-Aug. 1987, pp. 286-298.

9. CEB-FIP, "CEB-FIP Model Code 1990 Design Code," Comité Euro-International du Béton, 1990, 437 pp.

10. Banthia, N., and Trottier, J.-F., "Concrete Reinforced with Deformed Steel Fibers, Part I: Bond-Slip Mechanisms," *ACI Materials Journal*, V. 91, No. 5, Sept.-Oct. 1994, pp. 320-348.

11. Ouyang, C.; Pacios, A.; and Shah, S. P., "Pullout of Inclined Fibers from Cementitious Matrix," *Journal of Engineering Mechanics*, ASCE, V. 120, No. 12, Dec. 1994, pp. 2641-2659.

12. Lee, G. G., and Foster, S. J., "Behavior of Steel Fibre Reinforced Mortar in Shear III: Variable Engagement Model II," *Uniciv Report No. R-448*, School of Civil and Environmental Engineering, The University of New South Wales, Sydney, Australia, Sept. 2007, 86 pp.

13. Sujivorakul, C.; Waas, A. M.; and Naaman, A. E., "Pullout Response of a Smooth Fiber with an End Anchorage," *Journal of Engineering Mechanics*, ASCE, V. 126, No. 9, Sept. 2000, pp. 986-993.

14. Aveston, J., and Kelly, A., "Theory of Multiple Fracture of Fibrous Composites," *Journal of Materials Science*, V. 8, 1973, pp. 352-362.

15. Li, V. C.; Wang, Y.; and Backer, S., "A Micromechanical Model of Tension-Softening and Bridging Toughening of Short Random Fiber Reinforced Brittle Matrix Composites," *Journal of the Mechanics and Physics of Solids*, V. 39, No. 5, 1991, pp. 607-625.

16. Romualdi, J. P., and Mandel, J. A., "Tensile Strength of Concrete Affected by Uniformly Distributed and Closely Spaced Short Lengths of Wire Reinforcement," ACI JOURNAL, *Proceedings* V. 61, No. 6, June 1964, pp. 657-671.

17. Soroushian, P., and Lee, C.-D., "Distribution and Orientation of Fibers in Steel Fiber Reinforced Concrete," *ACI Materials Journal*, V. 87, No. 5, Sept.-Oct. 1990, pp. 433-439.

18. Soroushian, P., and Lee, C.-D., "Tensile Strength of Steel Fiber Reinforced Concrete: Correlation with Some Measures of Fiber Spacing," *ACI Materials Journal*, V. 87, No. 6, Nov.-Dec. 1990, pp. 541-546.

19. Stroeven, P., "Stereological Principles of Spatial Modeling Applied to Steel Fiber-Reinforced Concrete in Tension," *ACI Materials Journal*, V. 106, No. 3, May-June 2009, pp. 213-222.

20. Gettu, R.; Gardner, D. R.; Saldívar, H.; and Barrangán, B. E., "Study of the Distribution and Orientation of Fibers in SFRC Specimens," *Materials and Structures*, V. 38, Jan.-Feb. 2005, pp. 31-37.

21. Lee, S.-C.; Cho, J.-Y.; and Vecchio, F. J., "Diverse Embedment Model for Steel Fiber-Reinforced Concrete in Tension: Model Verification," *ACI Materials Journal*, V. 108, No. 5, Sept.-Oct. 2011, pp. 526-535.